Hierarchical $BiVO_4$ micro/nanostructures synthesised via a solvothermal route and photodegradation of Rhodamine B

Lin Ma, Li-Mei Xu, Ling-Ling Zhang

Chemistry Science and Technology School, Institute of Physical Chemistry, Zhanjiang Normal University, Zhanjiang 524048, People's Republic of China
E-mail: ma_lin75@126.com

Published in Micro & Nano Letters; Received on 8th March 2014; Revised on 19th April 2014; Accepted on 4th June 2014

Various bismuth vanadate ($BiVO_4$) hierarchical micro/nanostructures with cocoon-like, flower-like and branch-like morphologies were successfully synthesised by a facile template-free solvothermal approach. The as-synthesised products were characterised by X-ray diffraction, transmission electron microscopy (TEM), high-resolution TEM, scanning electron microscopy, nitrogen adsorption–desorption and UV–vis absorption spectroscopy. The experimental results indicate that the volume ratio of ethylene glycol to water has a remarkable influence on the morphologies and microstructures of the obtained products. An oriented aggregation process is presented to account for the formation of the hierarchical $BiVO_4$ micro/nanostructures in the current synthetic condition. In addition, the photocatalytic activity of the obtained $BiVO_4$ products under visible-light irradiation was initially evaluated by degradation of Rhodamine B.

1. Introduction: Inorganic micro/nanostructures with controllable and uniform sizes and shapes have attracted much attention because of their unique size- and shape-dependent properties and wide potential applications [1, 2]. Bismuth vanadate ($BiVO_4$) is a typical ternary semiconductor compound with a layered structure, which has gradually become a promising photocatalyst under visible light owing to its suitable bandgap energy ($E_g = 2.4$ eV), non-toxicity as well as chemical stability [3]. $BiVO_4$ exists in three polymorphs, namely tetragonal zircon, monoclinic scheelite and tetragonal scheelite, among which the monoclinic scheelite $BiVO_4$ (m-$BiVO_4$) is the most active photocatalytically under visible-light irradiation [4]. In addition, hierarchical structures have been attracting researchers' attention owing to their important role in the systematic study of structure–property relationships and their improved physical and chemical properties over their single components, and have been found to play a significant role in the photocatalytic performance of some photocatalysts [5–7]. It is considered that hierarchical structures can enhance the capture efficiency of incident light and the transfer rate of reactant molecules and provide more active sites [6, 7]. Recently, a variety of approaches such as the sol–gel method [6], liquid precipitation [8] and hydrothermal treatment [9–14] have been reported for synthesising micro/nanosized $BiVO_4$ with hierarchical structures. To obtain these desired micro/nanostructures, organic additives (surfactants, polymers and chelating agents) were generally employed to modify microstructures [9–14]. A few additive-free or template-free strategies have been successfully developed [15–17]. In view of the strong correlation between the properties of $BiVO_4$ and its morphology, structure and size, it is of great significance to find an effectively controllable synthesis of desired hierarchical structures.

In this Letter, a facile template-free solvothermal route is reported for the controlled fabrication of monoclinic $BiVO_4$ with various hierarchical architectures in ethylene glycol/H_2O mixed solvent. The effect of the volume ratio of ethylene glycol (EG) to water on the morphologies of the $BiVO_4$ products was investigated. In addition, the photocatalytic activity of the obtained $BiVO_4$ products under visible-light irradiation was initially evaluated by degradation of Rhodamine B.

2. Experimental details: A typical synthetic procedure for cocoon-like $BiVO_4$ was as follows: 1 mmol of NH_4VO_3 and 1 mmol of $Bi(NO_3)_3{\cdot}5H_2O$ were dissolved into 10 ml of deionised water and 30 ml of EG to form solutions A and B, respectively. The volume ratio of EG to water was 3:1. Then solution B was dropped into solution A under stirring. An orange suspension was formed. Afterwards, the suspension was transferred into a 50 ml Teflon-lined stainless steel autoclave. It was sealed tightly and maintained at 160°C for 16 h. After that, the autoclave was allowed to cool down naturally. Yellow precipitates were collected, and washed three times using deionised water and absolute ethanol and then dried for 12 h under vacuum at 60°C. For convenience, the obtained cocoon-like $BiVO_4$ sample was termed as c-$BiVO_4$. In addition, flower-like, branch-like and sheet-like $BiVO_4$ were also prepared by a similar synthetic route with different volume ratios of EG to water such as 1:1, 1:3 and 0:1, which were denoted as f-BiVO4, b-BiVO4 and s-$BiVO_4$, respectively.

The products were characterised by X-ray diffraction (XRD) (D/Max-2550), transmission electron microscopy (TEM) (JEOL JEM-2010F) and field-emission scanning electron microscopy (FE-SEM) (FEI SIRION-100). The nitrogen adsorption–desorption was conducted at 77 K on a Quantachrome NOVA 2000e sorption analyser (USA), and the Brunauer-Emmett-Teller surface area was estimated from the adsorption data. The absorption spectrum was measured on a UV–vis spectrophotometer (UV-2550) in the wavelength range of 300–700 nm. The photocatalytic performances of the $BiVO_4$ products were evaluated by the degradation of Rhodamine B under visible-light irradiation, which was provided by a 500 W high-pressure Xe lamp with a 420 nm cutoff filter. 22 mg of $BiVO_4$ photocatalyst was added into 10 ml of 8.6 mg/l Rhodamine B aqueous solution. Before irradiation, the suspension was sonicated for 15 min followed by continuous stirring for 1 h in the dark to ensure even dispersion of the photocatalyst and to allow the establishment of an adsorption–desorption equilibrium.

3. Results and discussion: Fig. 1*a* depicts the XRD pattern of the obtained c-$BiVO_4$ sample, which shows that the major detectable diffraction peaks can be easily attributed to the pure monoclinic phase of $BiVO_4$, matching well with the standard powder diffraction of $BiVO_4$ (JCPDS 14-0688). No impurity phase can be found, which confirms the high purity of the samples. The high and sharp peaks indicate that the c-$BiVO_4$ samples are well crystallised despite the slightly broadened peaks arising from the

© The Institution of Engineering and Technology 2014

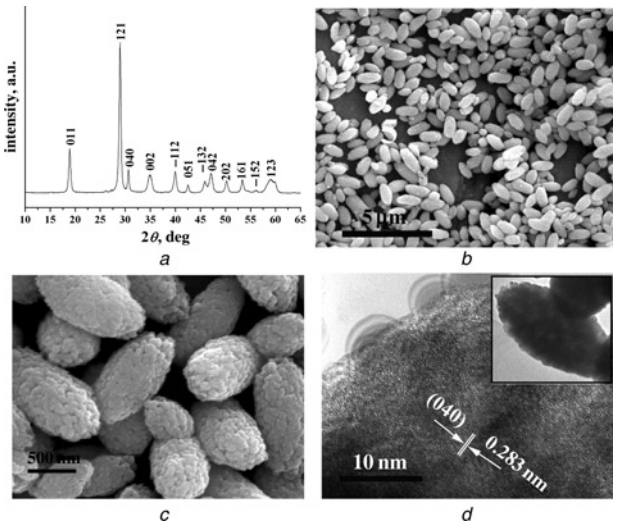

Figure 1 *XRD pattern (Fig. 1a), SEM images (Figs. 1b and c), and TEM image (Fig. 1d) of as-prepared c-$BiVO_4$ products with volume ratio of EG to water of 3:1*

nanostructured phases. Fig. 1*b* provides a typical SEM image of the c-$BiVO_4$ samples, which clearly displays a well-dispersed distribution of cocoon-like particles with uniform sizes and high yields. It is estimated that c-$BiVO_4$ particles have an average length of 1.21 μm and a mean width of 610 nm (aspect ratio ~2:1). The surface features of these cocoon-like particles were carefully inspected by a higher-resolution SEM image as shown in Fig. 1*c*. It can be seen that the surfaces of these cocoon-like particles are quite rough and covered with numerous nanoparticles. The microstructures of the c-$BiVO_4$ were further investigated by TEM and HRTEM techniques. The HRTEM image (Fig. 1*d*) shows lattice fringes with a *d*-spacing of 0.283 nm, in agreement with the (400) crystal planes of monoclinic $BiVO_4$. In addition, the inset of Fig. 1*d* also displays a well-defined cocoon-like particle with some tiny voids inside, which can be detected as reflected by the distinct bright/dark contrast. According to TEM and SEM observations, it is suggested that these cocoon-like $BiVO_4$ particles are assembled by numerous small nanoparticles in a certain way.

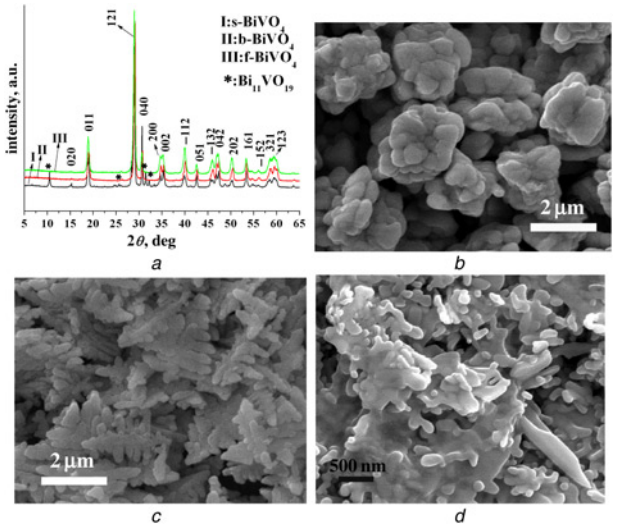

Figure 2 *XRD pattern (Fig. 2a), and SEM images of as-prepared f-$BiVO_4$ (Fig. 2b), b-$BiVO_4$ (Fig. 2c) and s-$BiVO_4$ (Fig. 2d) products with volume ratio of EG to water of 1:1, 1:3 and 0:1, respectively*

Control experiments were also conducted to investigate the effect of the volume ratio of EG to water on the morphology and structure of $BiVO_4$ products. It can be seen from Fig. 2*a* that the major detectable diffraction peaks are still indexed to the monoclinic phase of $BiVO_4$ (JCPDS 14-0688) except that traces of cubic $Bi_{11}VO_{19}$ are found as a byproduct for s-$BiVO_4$. Figs. 2*b–d* display the morphological evolution of the $BiVO_4$ products prepared with various volume ratios of EG to water. When the volume ratio of EG to water drops to 1:1, no cocoon-like $BiVO_4$ particles are observed. The resulting products present a hierarchical flower-like morphology. It is also discerned that these flower-like f-$BiVO_4$ products are composed of dozens of non-uniform particles with large sizes as petals. With further decrease of the volume ratio of EG to water to 1:1, the obtained products exhibit another branch-like architecture, completely distinct from the above morphologies. It is found that the b-$BiVO_4$ products are constructed from many branches perpendicularly growing on the major stem with a symmetrical arrangement. When pure water is used as the sole solvent, the resulting products are irregular rag-like sheets. The contrastive results indicate that the volume ratio of EG to water has a tremendous influence on the morphology of $BiVO_4$micro/nanostructures. In addition, N_2 adsorption–desorption measurements were performed to estimate the surface areas of the obtained products. It was calculated that the surface areas of the c-$BiVO_4$, f-$BiVO_4$ and b-$BiVO_4$ were 12.08, 6.52 and 1.82 m^2/g, respectively.

Based on the experimental results as well as previous reports [17–19], the probable formation process of the varied $BiVO_4$ nanostructures prepared with different volume ratios of EG to water in our current experiment can be preliminarily illustrated as shown in Fig. 3. As an efficient chelator for metal ions, it was easy for EG to chelate Bi^{3+} to form Bi^{3+}-EG complexes. Under solvothermal conditions, Bi^{3+} ions were continuously supplied at an appropriate rate by dissociation of the complexes. The dissociated Bi^{3+} ions could react with VO_4^{3-} to form $BiVO_4$ primary colloidal nanoparticles. These newborn primary particles would further grow into various secondary particles resulting from the difference between the growth rates of crystal planes in different EG/water systems possibly owing to the capping effect of EG. Table 1 provides the crystallite sizes of crystal planes of the products prepared with different EG/water systems. It can be seen from the crystallite sizes in Table 1 that the growth rates of the (121), (040), (002) and (−112) planes increase, while the growth rate of (011) decreases with the increase of the volume ratio of EG to water. Afterwards, these secondary particles aggregated together to minimise their surface energy in an oriented way and further grew to form the final products under solvothermal conditions. In different EG–water environments, the different viscosities of the solvent might allow $BiVO_4$ secondary particles to find different low-energy configuration interfaces because of different viscosities and thus aggregated in a disparate oriented way [19]. The detailed formation mechanism of these $BiVO_4$ hierarchical micro/nanostructures deserves further investigations.

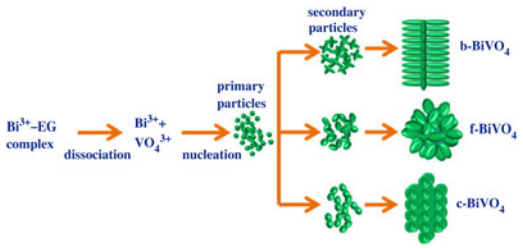

Figure 3 *Illustration of formation process of varied $BiVO_4$ micro/nanostructures via an oriented aggregating way under solvothermal conditions*

© The Institution of Engineering and Technology 2014

doi: 10.1049/mnl.2014.0128

Table 1 Crystallite sizes of various crystal planes of obtained products

Sample	(011) crystallite sizes, nm	(121) crystallite sizes, nm	(040) crystallite sizes, nm	(002) crystallite sizes, nm	(−112) crystallite sizes, nm
c-$BiVO_4$	20.8	21.4	31.0	10.4	16.1
f-$BiVO_4$	20.1	24.1	31.2	10.9	16.4
b-$BiVO_4$	18.9	28.3	39.1	13.3	18.0

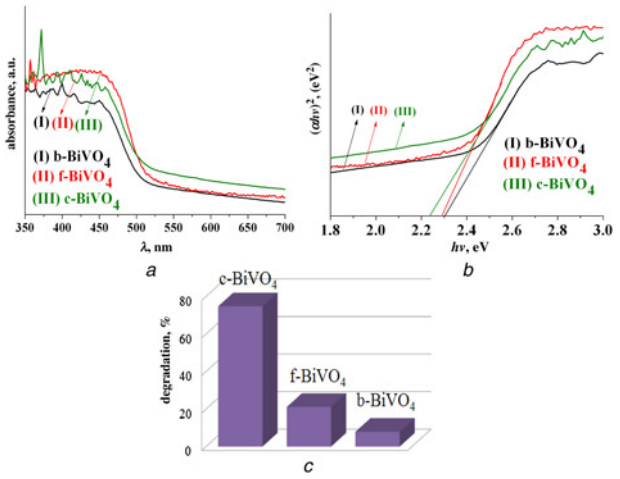

Figure 4 *UV–vis diffuse reflectance spectra (Fig. 4a), calculation diagram of their bandgaps (Fig. 4b), and column diagram of photocatalytic degradation of Rhodamine B under visible-light irradiation of $BiVO_4$ products (Fig. 4c)*

Fig. 4*a* shows the UV–vis absorption spectra of the different $BiVO_4$ products prepared with different volume ratios of EG to water via a solvothermal process, which displays the photoabsorption property from the UV light region to the visible-light region. It can be seen that all $BiVO_4$ products exhibit strong absorption in the visible range, indicating that they are potentially good photocatalysts for sunlight-driven applications. Moreover, a slight red shift of the absorption edge can also be discerned with increasing ratios of EG to water. As a crystalline semiconductor, the optical absorption near the band edge is based on the equation $\alpha h\nu = A(h\nu - E_g)^{1/2}$ (where α is the absorption coefficient, A is a constant, $h\nu$ is the photo energy and E_g is the bandgap). From the curve of the $(\alpha h\nu)^2$ against photo energy ($h\nu$), the bandgaps were estimated to be about 2.31, 2.29 and 2.23 eV, corresponding to the b-$BiVO_4$, f-$BiVO_4$ and c-$BiVO_4$ products, respectively, which are slightly lower than or similar to those of the $BiVO_4$ materials reported previously [9–14]. The photocatalytic degradation activities of the $BiVO_4$ products are shown in Fig. 4*b*. After a 120 min degradation process, the degradation rates for Rhodamine B are 74.8, 21.1 and 7.9%, respectively, for the c-$BiVO_4$, f-$BiVO_4$ and b-$BiVO_4$ products. Amongst the three products, c-$BiVO_4$ exhibits the best photocatalytic performance for Rhodamine B degradation, which might be attributed to its relatively large aspect surface areas, narrow bandgap, uniform morphologies and small crystallite sizes.

4. Conclusion: In brief, monoclinic $BiVO_4$ hierarchical micro/nanostructures with various morphologies such as cocoon-like, flower-like and branch-like have been synthesised via a facile template-free solvothermal route. The results revealed that the morphologies and microstructures of the final products were strongly influenced by the volume ratio of EG to water. The formation of the hierarchical structures could be attributed to an oriented aggregation by nanoparticles under our solvothermal process. In addition, during photocatalytic degradation of Rhodamine B, the cocoon-like $BiVO_4$ product demonstrated the best visible-light photocatalytic activity, which possibly resulted from its relatively large aspect surface areas, narrow bandgap, uniform morphologies and small crystallite sizes.

5. Acknowledgments: This work was financially supported by the Guangdong Natural Science Foundation for Ph.D. Start-up Research Program (no. 10452404801004521).

6 References

[1] El-Sayed M.A.: 'Some interesting properties of metals confined in time and nanometer space of different shapes', *Acc. Chem. Res.*, 2001, **34**, (4), pp. 257–264
[2] Alivisatos A.P.: 'Semiconductor clusters, nanocrystals, and quantum dots', *Science*, 1996, **271**, (5251), pp. 933–937
[3] Kudo A., Omori K., Kato H.: 'A novel aqueous process for preparation of crystal form-controlled and highly crystalline $BiVO_4$ powder from layered vanadates at room temperature and and its photocatalytic and photophysical properties', *J. Am. Chem. Soc.*, 1999, **121**, (49), pp. 11459–11467
[4] Tokunaga S., Kato H., Kudo A.: 'Selective preparation of monoclinic and tetragonal $BiVO_4$ with scheelite structure and their photocatalytic properties', *Chem. Mater.*, 2001, **13**, (12), pp. 4624–4628
[5] Kuang D.B., Brezesinski T., Smarsly B.: 'Hierarchical porous silica materials with a trimodal pore system using surfactant templates', *J. Am. Chem. Soc.*, 2004, **126**, (34), pp. 10534–10535
[6] Parlett C.M.A., Wilson K., Lee A.F.: 'Hierarchical porous materials: catalytic applications', *Chem. Soc. Rev.*, 2013, **42**, (9), pp. 3876–3893
[7] Cho K., Na K., Kim J., Terasaki O., Ryoo R.: 'Zeolite synthesis using hierarchical structure-directing surfactants: retaining porous structure of initial synthesis gel and precursors', *Chem. Mater.*, 2012, **24**, (14), pp. 2733–2738
[8] Yin C., Zhu S.M., Chen Z.X., Zhang W., Gu J.J., Zhang D.: 'One step fabrication of C-doped $BiVO_4$ with hierarchical structures for a high-performance photocatalyst under visible light irradiation', *J. Mater. Chem. A*, 2013, **1**, (29), pp. 8367–8378
[9] Meng X., Zhang L., Dai H.X., Zhao Z.X., Zhang R.Z., Liu Y.X.: 'Surfactant-assisted hydrothermal fabrication and visible-light-driven photocatalytic degradation of methylene blue over multiple morphological $BiVO_4$ single-crystallites', *Mater. Chem. Phys.*, 2011, **125**, (1–2), pp. 59–65
[10] Jiang H.Y., Meng X., Dai H.X., *ET AL.*: 'High-performance porous spherical or octapod-like single-crystalline $BiVO_4$ photocatalysts for the removal of phenol and methylene blue under visible-light illumination', *J. Hazard. Mater.*, 2012, **217–218**, pp. 92–99
[11] Zhu Z.F., Du J., Li J.Q., Zhang Y.L., Liu D.G.: 'An EDTA-assisted hydrothermal synthesis of $BiVO_4$ hollow microspheres and their evolution into nanocages', *Ceram. Int.*, 2012, **38**, (6), pp. 4827–4834
[12] Fan H.M., Wang D.J., Wang L.L., *ET AL.*: 'Hydrothermal synthesis and photoelectric properties of $BiVO_4$ with different morphologies: an efficient visible-light photocatalyst', *Appl. Surf. Sci.*, 2011, **257**, pp. 7758–7762
[13] Li J.Q., Wang D.F., Liu H., Du J., Zhu Z.F.: 'Nanosheet-based $BiVO_4$ hierarchical microspheres and their photocatalytic activity under visible light', *Phys. Status Solidi A*, 2012, **209**, (2), pp. 248–253
[14] Lu Y., Luo Y.S., Kong D.Z., Zhang D.Y., Jia Y.L., Zhang X.W. : 'Large-scale controllable synthesis of dumbbell-like $BiVO_4$ photocatalysts with enhanced visible-light photocatalytic activity', *J. Solid State Chem.*, 2012, **186**, pp. 255–260
[15] Ren L., Jin L., Wang J.B., Yang F., Qiu M.Q., Yu Y.: 'Template-free synthesis of $BiVO_4$ nanostructures: I. Nanotubes with hexagonal cross sections by oriented attachment and their photocatalytic property for water splitting under visible light', *Nanotechnology*, 2009, **20**, (11), pp. 115603–115611
[16] Zhao Y., Xie Y., Zhu X., Yan S., Wang S.X.: 'Surfactant-free synthesis of hyperbranched monoclinic bismuth vanadate and its applications in photocatalysis, gas sensing, and lithium-ion batteries', *Chem. Eur. J.*, 2008, **14**, (5), pp. 1601–1606

© The Institution of Engineering and Technology 2014

[17] Wang X.J., Liu H.L., Wan X.L., Wang J.R., Chang L.L. : 'Additive-free solvothermal synthesis of peanut-like $BiVO_4$ powders with enhanced photocatalysis activity', *Cryst. Res. Technol.*, 2013, **48**, (12), pp. 1066–1072
[18] Wang X.K., Li G.C., Ding J., Peng H.R., Chen K.Z.: 'Facile synthesis and photocatalytic activity of monoclinic $BiVO_4$ micro/nanostructures with controllable morphologies', *Mater. Res. Bull.*, 2012, **47**, (11), pp. 3814–3818
[19] Ge M., Liu L., Chen W., Zhou Z.: 'Sunlight-driven degradation of Rhodamine B by peanut-shaped porous $BiVO_4$ nanostructures in the H_2O_2-containing system', *Cryst. Eng. Commun.*, 2012, **14**, (3), pp. 1038–1044

© The Institution of Engineering and Technology 2014

doi: 10.1049/mnl.2014.0128